

Materials and Methods

Cloning, protein expression and purification

The full-length gene of sTeLIC was codon optimized for expression in *E. coli* and chemically synthesized. The N-terminus of sTeLIC was fused to an MBP tag with a thrombin protease cleavage site. The recombinant gene was subcloned into the pET20b vector. The primers used to amplify the full-length sTeLIC are:

Forward primer:

5-CGACGTGCGGCCGCGATGGCAAGCCTGGCAGCAG-3

Reverse primer:

5-CTCGAGCTAATAGCTACGCCAAAAAACAGCC-3

The plasmid containing the recombinant gene was transformed into *E. coli* C43 competent cells. The medium used to express the recombinant protein was 2YT. 1 mM ampicillin was added during cell culture and protein expression. The temperature was decreased from 37°C to 20°C when the optical density (OD) reached 0.6-0.8, with the addition of 0.4 mM isopropyl β -D-1-thiogalactopyranoside (IPTG) for overnight induction. The overnight culture was harvested and the pellet was suspended using buffer A (20mM Tris pH 8.0, 300 mM NaCl) supplemented with EDTA-free protease inhibitor (ThermoFisher) and Benzonase nuclease. Cells were disrupted by sonication and subsequently spun at 40,000 rpm for 1 h. The pellet was collected and dissolved using buffer A containing 4% n-dodecyl- β -D-maltoside (DDM) at 4°C for 3 h. The dissolved membranes were then spun at 28,000 rpm for 1 h. The supernatant was applied to an amylose resin (New England BioLabs) which was equilibrated with buffer A. Incubation of the supernatant with amylose resin was limited to around half an hour in order to avoid introduction of a contaminant, maltoporin. The amylose resin was extensively washed with buffer A containing 0.1% DDM followed by buffer B (buffer A containing 0.02% DDM). Recombinant protein was then eluted by buffer B containing 50 mM D-(+)-maltose monohydrate (Sigma), subsequently concentrated, and applied to a Superose TM6 Increase 10/300 GL (GE Healthcare) gel filtration column, which was pre-equilibrated with buffer B. The fractions of the peak corresponding to a molecular weight of five times MBP-sTeLIC were pooled and concentrated. The MBP tag was removed by incubating with thrombin protease overnight. MBP and thrombin were then removed from the solution by another round of gel filtration in buffer B. The fractions of the peak

corresponding to the sTeLIC pentamer were pooled and concentrated to 12 mg/ml. All the purification steps were handled at 4°C. Protein was frozen and stored at -80°C for further use.

Crystallization and data collection

Crystallization experiments were set up at 18°C. The purified protein in buffer B was mixed with an equal volume of the reservoir buffer containing 100 mM Tris pH 8.0, 150 mM MgCl₂, 3% DMSO, and 32% PEG 200 at 1 μ l: 1 μ l volume ratio and the drops were equilibrated against a 1 ml reservoir solution using the hanging drop method. The pH of the drop, around pH 8.0, was checked using pH strips. Crystals appeared after two days and grew to full size after around two weeks. For reproducibility, and in order to get larger crystals, the purified protein was mixed with 65 mM NDG at 4:1 volume ratio and incubated on ice for 20 min prior to crystallization set-up. Micro-seeding procedure was additionally applied to increase the reproducibility of the crystals.

Co-crystallization of sTeLIC with 4-BrC was performed by mixing the protein with 4-BrC at a final concentration of 3 mM (solubilized in 100% DMSO) and incubating at 4°C overnight. Crystals of the sTeLIC with 4-BrC appeared within two weeks and grew to full size within a month using the same method and the same mother liquor as described above.

Soaking experiments of sTeLIC crystals with Br⁻, Cs⁺, and Ba⁺⁺ ions entailed incubation with mother liquor supplemented with 100 mM KBr, 150 mM CsCl, and 150 mM BaCl₂, for 5-30 min respectively.

Crystals were flash frozen in liquid nitrogen. Diffraction data sets were collected at ESRF (beamline ID23-2 and ID29) or Soleil (Proxima1 and Proxima2) and processed using XDS¹ and CCP4² software. The crystals belong to C2 space group with one pentamer in the asymmetric unit.

Structure determination and model refinement

The structure was solved by molecular replacement using GLIC (PDB ID: 4HFI) as the search model by Phaser-MR in Phenix³. Before molecular replacement, the PDB file of GLIC was modified by the program Chainsaw in CCP4, keeping the side chains atoms if the residues are the same, otherwise truncating the side-chain of the model to the C-beta atom. The

result of the molecular replacement gave Log-Likelihood-Gain and top translation-function Z-score values of 282 and 10.3 respectively. The refinement was performed using Buster⁴, alternating cycles of refinement and manual building in Coot⁵. During the refinement, auto non-crystallographic symmetry (NCS) restraints were applied. We also used the five-fold averaged NCS map to trace the chains during model building. There are 25 methionines in the sTeLIC pentamer (five in each monomer, omitting the first one), therefore we collected one diffraction data set at the sulfur edge (1.7 Å). Taking advantage of the anomalous signal coming from sulfur, we confirmed the correct assignment of the protein sequence in the model. The best data set of sTeLIC was crystallized with NDG and processed at 2.3 Å resolution. Clear electron-density coming from NDG can be seen on the surface of the ion channel pore in the TMD. One NDG molecule was assigned for each monomer with the sugar head facing the ion channel pore and its curly alkyl tail inserted into the hydrophobic cleft formed by two adjacent subunits. The final model contains residues ranging from Glu7 to Phe316, missing only six N-terminal and four C-terminal residues. 662 water molecules were built into the model. Model quality was assessed in Coot⁵ and by Molprobit⁶. 97.66% residues fall into the preferred regions of the Ramachandran plot and the rest (2.34%) fall into the allowed regions.

The best data set of sTeLIC with 4-BrC was collected at 0.873 Å wavelength. The crystal was isomorphous to the native one. Taking advantage of the anomalous signal coming from the bromine atom, we could build the 4-BrC molecule into the model without ambiguity. Sequence alignment was done using ClustalW2⁷ and represented using ESPript⁸. Structural analysis and comparison were done by Pymol⁹ and Chimera¹⁰. The surface electrostatic potential map was generated by APBS server¹¹s and read by Chimera¹². HOLE software¹³ was used to analyze the channel pore dimensions. Pictures were prepared by Pymol and Chimera.

Oocyte injection and incubation

Xenopus laevis oocytes were obtained from the Centre de Ressources Biologiques–Rennes, France. Defolliculated oocytes were maintained at 4°C in a modified Barth's saline solution (88 mM NaCl, 1 mM KCl, 0.8 mM MgSO₄, 2.4 mM NaHCO₃, 0.3 mM NaNO₃, 15 mM HEPES/Na pH

8) with 0.7 mM CaCl₂. After intra-nucleus injection of ~30 nL cDNA (80 ng/μl specified clone cDNA with 20 ng/μl of GFP cDNA), using a compressed air microinjection system, the oocytes were transferred to 18°C. 1-2d later they were evaluated for GFP expression, and subsequently maintained at 15°C.

Immunolabeling

sTeLIC-WT, sTeLIC-D227A, or mock injected oocytes were fixed in 4% paraformaldehyde (4°C, O/N), washed in phosphate buffered saline ([PBS] 137 mM NaCl, 2.7 mM KCl, 5.3 mM Na₂HPO₄, 1.5 mM KH₂PO₄ pH 7.4 for 30min, at room temperature [RT]), blocked in PBS + 4% horse serum (30 min, RT [Sigma Aldrich]), and immunolabeled using a rabbit anti-HA tag primary antibody (2.5 μg/ml for 1.5 hr, [Sigma Aldrich]), and a goat anti-rabbit AlexaFluor-647 coupled secondary antibody (10 μg/ml for 1 hr, RT [ThermoFisher Scientific]), both in PBS + 2% horse serum with a 5 min rinse of the same solution before, inbetween, and after antibody applications. Oocytes were then fixed again with 4% paraformaldehyde (4°C, O/N), placed into blocks of 3% low-melting agarose in PBS, stored at 4°C, and subsequently sliced at 40 μm intervals. Slices of three different oocytes per construct were placed onto slides and fixed using the ProLong Diamond antifade mountant with DAPI (ThermoFisher) and analyzed using fluorescence microscopy with constant exposure times using GFP and Cy5 filters.

Two-electrode Voltage Clamp Electrophysiology

Recordings were made 1-5d after oocyte injection using low-resistance (0.2-2 MΩ) electrodes filled with 3 M KCl, and clamping the voltage to -40 mV unless otherwise specified. The standard solution superfusing the oocyte during recording at room temperature was 100 mM NaCl, 3 mM KCl, 1 mM MgCl₂, 1 mM CaCl₂, 10 mM HEPES pH 7.5 using NaOH. Any subsequent reference to standard-solution uses this formulation, at pH 7.5 unless otherwise stated. NaOH was used to obtain desired pHs of other HEPES solutions unless otherwise specified. Overall, two main protocols were used for sTeLIC activation in this report. Most oocyte experiments were performed using washes/recovery in standard-solution with tests in CaCl₂-free standard-solution, both at pH 7.5 (part of **Suppl. Table S2**, as well as **Suppl. Table S3**, **Fig. 5A-B**, **Suppl. Fig. S8**, and

Suppl. Fig. S11). The most recent experiments were performed in CaCl₂-free standard-solution, with washes/recovery at pH 5, and tests at pH 8 (**Fig. 4A-B**, **Fig. 5C**, **Fig. 7**, and **Suppl. Fig. S10**), or at various pHs (**Fig. 1**). A wash in a solution either with 1 mM CaCl₂ or at pH 5 was necessary to restore sTeLIC ability to be activated. A detailed description of the protocols used follows:

Evaluation of compound effects (Suppl. Table S2) without and with a potentiator was performed using the specified test concentration in either the standard-solution or CaCl₂-free standard-solution, and the standard-solution containing 30 mM MES or CaCl₂-free standard-solution containing 10 μM 4-BrC, respectively.

Evaluation of the potentiation of currents by compounds (Suppl. Table S3 and Fig. 5A-B) was performed using CaCl₂-free standard-solution superfused for 30 sec before and after applications of the compound at the specified concentration also in CaCl₂-free standard-solution for 15 sec-1 min depending on compound. The wash time, using the standard-solution, was 15 min in-between sweeps. An initial test pulse to ensure receptor expression was performed using the maximum concentration followed by a 15 min wash before the recording of sweeps. A total of 6 sweeps per curve, in either ascending or descending concentration, was conducted on an individual oocyte. MES was applied for 1-3 min, after 30 sec in CaCl₂-free standard-solution, and was then washed directly using standard-solution for varying times.

Evaluation of currents at different pHs (Fig. 1A-B) was tested in either 10 mM HEPES or 10 mM Tris CaCl₂-free solutions (100 mM NaCl, 3 mM KCl, 1 mM MgCl₂). The stock solution was raised to pH 10.5 using NaOH and subsequently lower pH's were obtained using HCl with possibly the addition of the pH 10.5 solution to obtain the desired pH, thereby maintaining an equivalent Na concentration in all solutions. All pH testing was performed in the absence of CaCl₂ throughout the entire experiment.

Desensitization experiments (Fig. 1C and Fig. 5C) were performed in CaCl₂-free standard solution with washes at pH 5.

Evaluation of ion selectivity (Fig. 4A-B) was performed using *N*-methyl-D-glucamine (NMDG) and HCl to obtain the desired pH of 10 mM

HEPES solutions (100 mM NaCl and 1 mM MgCl₂). Sorbitol was used to maintain the desired osmolarity, where solutions containing 0 mM NaCl contained 200 mM sorbitol. Neither of these compounds were found to have an effect upon the receptor (**Suppl. Fig. S10** for sorbitol). Ascending ramps (0.1 V/s) from -100 to +100 mV were applied every 5 sec for a minimum of five times, with a 100 ms hold at -100 mV before ramping and a return to -100 mV after the ascending ramp. A holding potential of -60 mV was maintained between ramps. The base-line measurements at pH 5 were subtracted from subsequent voltage ramp currents measured on the same oocyte.

Evaluation of divalent cation inhibition was initially performed using standard solution, where inhibition of 30 mM MES elicited current was measured with the addition of divalent ions at a concentration of 50 mM (CaCl₂ and MgCl₂) or 1 mM (BaCl₂ and ZnCl₂). Data corresponding to **Fig. 8A-C**, with IC₅₀ values for Zn⁺⁺, Ba⁺⁺, and Ca⁺⁺ inhibition, were obtained using washes in CaCl₂-free standard-solutions at pH 5, and pH 8 elicited currents. 1 min applications of pH 8 before and after a 1 min perfusion of the specified concentration of the divalent cation at pH 8 were subsequently followed by 2.5 min washes at pH 5.

Mg⁺⁺ inhibition was tested using pH 8 elicited currents, from control at pH 5, with the addition of 1 mM and 30 mM MgCl₂ to standard solution devoid of divalent ions, where only oocytes with a stable base-line were used for measurement (n=3).

Voltage-dependence of inhibition (**Fig. 8E-F**), tested at constant voltage, was examined in the same manner as the IC₅₀ experiments, using pH 8 elicited currents in CaCl₂-free standard-solution, but with the addition of 200 μM BaCl₂ or 5 μM ZnCl₂. Perfusion times were 60 sec, 90 sec, and 60 sec for activation, inhibition, and the return from inhibition, respectively, with 2.5 min wash times before and after pH 8 application. The entire sweep time was held at constant voltages ranging from -80mV to +40mV or +40mV to -80mV in 20mV increments for a total of at least three oocytes tested per cation. Several oocytes did not tolerate prolonged clamping at +40mV and therefore we excluded these values from our analysis. Voltage-dependence of inhibition was also tested in a voltage ramp protocol for Zn⁺⁺, Ba⁺⁺, and Ca⁺⁺ (**Fig. 8D**), where current-voltage relationships of pH 8 elicited current in the absence or presence

of 5 μM ZnCl_2 , 200 μM BaCl_2 , or 200 μM CaCl_2 added to CaCl_2 -free standard-solution were obtained similarly to the selectivity experiments. Ascending and descending ramps from either -100mV to +100mV or +100mV to -100mV at a rate of 0.02 V/s, to allow for ion dissociation, were completed on at least three oocytes each for each divalent cation. The results of representative descending ramps are shown in **Fig 8D**. The base-line measurements of pH5 CaCl_2 -free standard-solution was subtracted from both the pH 8 and the pH 8 + divalent ion measurements recorded on the same oocyte. The Erev calculations during these experiments varied quite greatly from -7 mV to +7 mV, and the appearance of a 'contaminating' current at positive potentials seen especially for Ca^{++} in **Fig 8D** was present for roughly half of the oocytes tested.

TMA, TEA, and TPA were tested at 50 mM using pH 8 CaCl_2 -free standard solution elicited currents, from control at pH 5 (n=3) (**Suppl. Fig. S11**), where activation times varied from 1 min-2 min, followed by addition of ammonium cation at pH 8 for 60 sec-2min, and a return to pH 8 solution for 1 min-2 min. TMA and TEA were also similarly tested at 50 mM with 50 μM 4-BrC in CaCl_2 -free standard solution.

Evaluation of recordings

For concentration-dependent responses of a compound A, the mean \pm standard deviation reported is the mean of the EC_{50} and Hill-slope values obtained for individually recorded oocytes. A sigmoidal dose-response fit to the peaks, calculated as:

$$\text{Response} = \text{Basal} + \frac{\text{Imax} - \text{Basal}}{1 + 10^{(\text{Log}(\text{EC}_{50}) - \text{Log}[\text{A}])^n}}, \quad \text{was}$$

used to obtain the EC_{50} (from the $\text{Log}[\text{EC}_{50}]$) and Hill-slope (n) for the set of concentrations ($\text{Log}[\text{A}]$) tested on an individual oocyte. Maximum (Imax) and minimum (Basal) refer to the absolute value of the inward (negative) current response.

For potentiation tests: peaks are calculated using the maximal response to CaCl_2 -free standard-solution subtracted from the overall maximum per sweep.

For pH tests: the holding current (at pH 5) before application of the desired pH is subtracted from the overall maximum per sweep.

For inhibition tests: the 'peak' is calculated as the minimum during cation application divided by the maximum obtained before cation application, where the leak current measured at the

beginning of the sweep is removed from both measurements. Fits were constrained to have a minimal value of 0.

The graphs in the tables show the mean \pm standard deviation of all normalized recorded peak currents for the specified concentrations, which are normalized to their recorded oocyte's maximal peak current, with one non-linear regression fit to all the data. These fits are not constrained. All calculations were made using GraphPad Prism 4 (GraphPad Software Inc.).

No leak subtraction was applied to display oocyte current traces in the figures, except in **Fig. 1C** upper trace (pH 8), where 0.06 μA was added to every current value in the trace.

sTeLIC expression in BHK cells

Cells of the tk-ts13 variant of the baby hamster kidney (BHK) cell line were grown at 37°C under a 5% CO_2 atmosphere, in Dulbecco – modified Eagle medium (DMEM) with 4.5 g/L glucose, pyruvate and Glutamax (In Vitrogen), supplemented with heat inactivated fetal calf serum (5 %). Petri dishes (35 mm in diameter) were transfected one day after cell plating, using a calcium phosphate – DNA co-precipitation method. A pMT3 plasmid containing the cDNA sequence of sTeLIC was mixed with a pMT3 plasmid coding for GFP, in quantities of 2 and 0.2 μg per 35 mm dish. GFP positive cells were used for electrophysiology 1-2d after transfection.

Outside-out and whole-cell patch-clamp recording.

Patch-clamp methods were updated from Van Renterghem and Lazdunski¹⁴. Voltage-clamp currents from BHK cell plasma membrane were recorded using an RK-400 patch-clamp amplifier (Bio-Logic, France) with an HK-R-410/08 dual resistor headstage. Computer acquisition and stimulation were done using the program pClamp 10 and a Digidata 1550 analogic/digital interface (Axon Instrument). The current signal was low-pass filtered at 1 kHz, and digitized at a sampling frequency of 40 kHz (outside-out patches, [o/o]) or 10 kHz (whole-cell [WC]). Digital filtering by 100 to 1 (and 10 to 1, respectively) data points averaging was further applied to display traces in **Fig 7** main trace (and **Inset**). Pipettes were pulled from thick wall (0.37 mm) borosilicate glass (1.5 mm o.d., 0.75 mm i.d.), and fire-polished to resistances of 5 to 7 $\text{M}\Omega$ (o/o) or 2-4 $\text{M}\Omega$ (WC) in our solutions.

For single-channel identification (Fig. 7), the pipette solution (intracellular face of the membrane) used was composed of: 155 mM NaCl, 1 mM MgCl₂, 10 mM BAPTA, 10 mM HEPES and NaOH to pH 7.5, and the solution superfused (extracellular face) was prepared with: 170 mM NaCl, 1 mM MgCl₂, 10 mM HEPES and NaOH to pH 9. Lower pH values (7.5 and 5.0) were reached by addition of HCl (2 M). The culture dish was rinsed and filled with this extracellular solution (pH 7.5) supplemented with 1 mM CaCl₂. Both wash and test solutions were at pH 7.5, but before stimulation, a 20 s pretreatment at pH 5 was applied in order to reverse desensitization/inactivation, with the addition of 30 μM 4-BrC to the pH 7.5 solution occurring 10 s after the end of the pretreatment.

For charge selectivity analysis (Fig. 4C-D), the pipette solution was composed of: 170 mM NaCl, 1 mM MgCl₂, 10 mM HEPES and NaOH to pH 7.5, and the extracellular solutions were prepared by mixing this solution with a solution of 340 mM sorbitol, 1 mM MgCl₂, and 10 mM HEPES adjusted to pH 7.5 using NaOH. Reversal potentials shown in Fig. 4D, as well as the P_{Cl}/P_{Na} values obtained from data in 17 mM NaCl, were calculated from the Goldman, Hodgkin, and Katz voltage equation using Na⁺ concentrations equal to the NaCl concentration plus 5 mM (from NaOH used to neutralize 10 mM HEPES up to pH 7.5), and Cl⁻ concentrations equal to the NaCl concentration plus 2 mM (from 1 mM MgCl₂). All ratios of activity coefficients were assumed to be equal to 1, which accounts for the largest source of error in the Erev measurements. No correction was applied for the pipette tip liquid-junction potential, since, starting with 170 mM NaCl

solutions without (pipette) and with (bath) 1 mM CaCl₂, it was expected to be very near 0 mV.

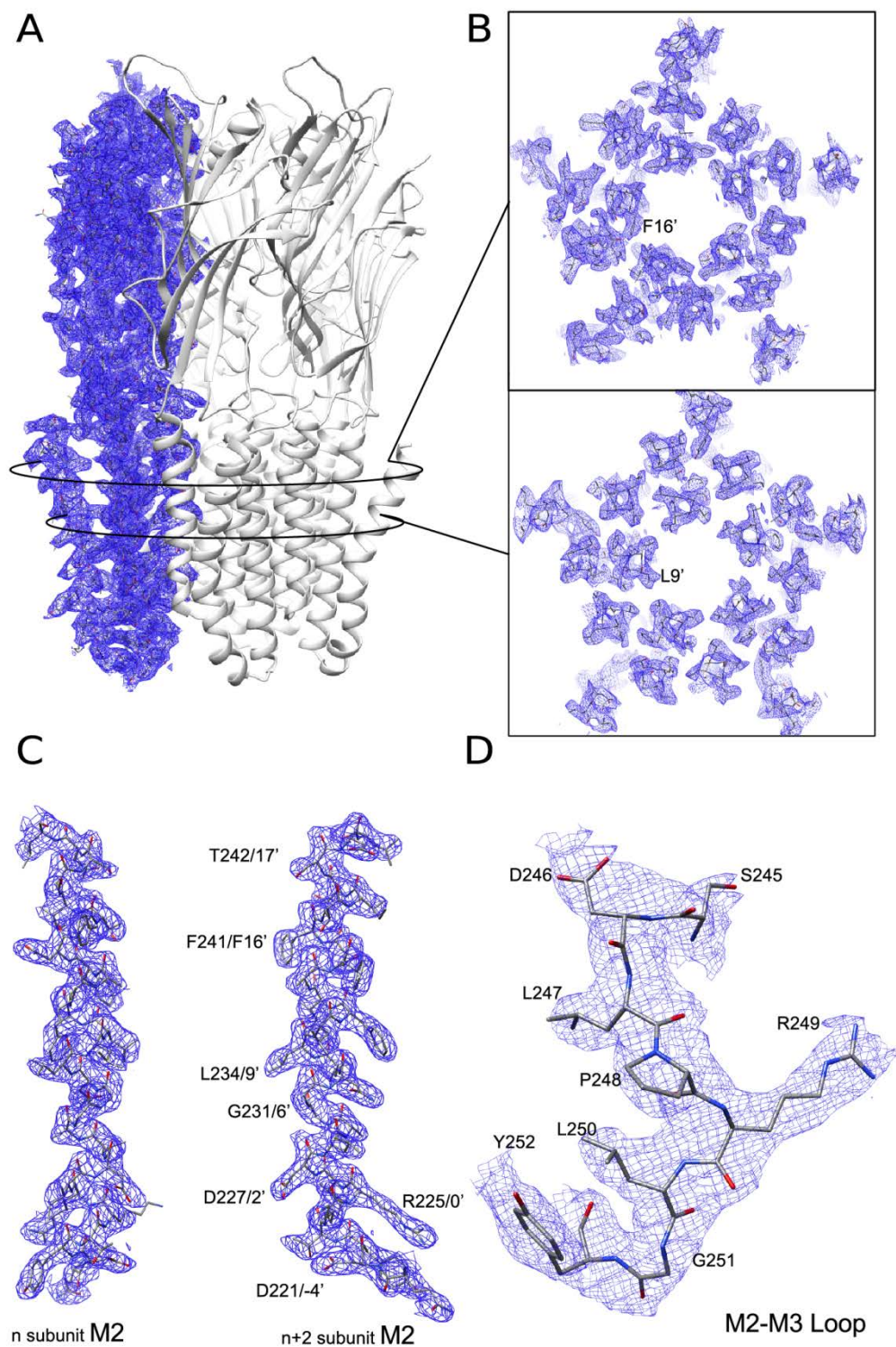
Selectivity data were collected from three whole-cell and two outside-out recordings, from a total of five cells. The extracellular solution was changed from 170 mM NaCl at pH 5.0 to a given NaCl concentration at pH 7.5, then, 10-20 s later, 30 μM 4-BrC was added and desensitization was allowed to occur. Ascending voltage ramps (0.4 V/s) from -100 to +100 mV were applied every 2 s. The reversal potential was stable during desensitization. For Erev measurements and establishment of sTeLIC current I-V curves (Fig. 4C), the average of three traces collected at the end of desensitization was subtracted from the average of two traces collected at the beginning of desensitization, in each condition. With this protocol, sTeLIC current reversal potential was measured at pH 7.5 in the presence of 30 μM 4-BrC.

Solutions were applied locally over the patch or the cell, using a gravity driven, multiway perfusion system converging to a single tip (50-100 μL/min). Liquid junction potentials, if any between locally perfused and bath solutions were not taken into account. A 3 M KCl, 5 g/L agar bridge was used to isolate the reference electrode from changes in the extracellular solution.

All transmembrane potential differences are given as intracellular minus extracellular potential values. For all voltage-clamp experiments, electric current flowing inward through the cell membrane is counted negative and represented downwards.

References of Materials and Methods

1. Kabsch, W. Integration, scaling, space-group assignment and post-refinement. *Acta Crystallogr. D Biol. Crystallogr.* **66**, 133–144 (2010).
2. Winn, M. D. *et al.* Overview of the CCP4 suite and current developments. *Acta Crystallogr. D Biol. Crystallogr.* **67**, 235–242 (2011).
3. Adams, P. D. *et al.* PHENIX: a comprehensive Python-based system for macromolecular structure solution. *Acta Crystallogr. D Biol. Crystallogr.* **66**, 213–221 (2010).
4. Blanc, E. *et al.* Refinement of severely incomplete structures with maximum likelihood in BUSTER-TNT. *Acta Crystallogr. D Biol. Crystallogr.* **60**, 2210–2221 (2004).
5. Emsley, P., Lohkamp, B., Scott, W. G. & Cowtan, K. Features and development of Coot. *Acta Crystallogr. D Biol. Crystallogr.* **66**, 486–501 (2010).
6. Chen, V. B. *et al.* MolProbity: all-atom structure validation for macromolecular crystallography. *Acta Crystallogr. D Biol. Crystallogr.* **66**, 12–21 (2010).
7. Thompson, J. D., Higgins, D. G. & Gibson, T. J. CLUSTAL W: improving the sensitivity of progressive multiple sequence alignment through sequence weighting, position-specific gap penalties and weight matrix choice. *Nucleic Acids Res.* **22**, 4673–4680 (1994).
8. Robert, X. & Gouet, P. Deciphering key features in protein structures with the new ENDscript server. *Nucleic Acids Res.* **42**, W320–W324 (2014).
9. PyMOL | www.pymol.org. Available at: <http://www.pymol.org/>. (Accessed: 9th July 2017)
10. Pettersen, E. F. *et al.* UCSF Chimera--a visualization system for exploratory research and analysis. *J. Comput. Chem.* **25**, 1605–1612 (2004).
11. Unni, S. *et al.* Web servers and services for electrostatics calculations with APBS and PDB2PQR. *J. Comput. Chem.* **32**, 1488–1491 (2011).
12. Baker, N. A., Sept, D., Joseph, S., Holst, M. J. & McCammon, J. A. Electrostatics of nanosystems: application to microtubules and the ribosome. *Proc. Natl. Acad. Sci. U. S. A.* **98**, 10037–10041 (2001).
13. Smart, O. S., Neduveilil, J. G., Wang, X., Wallace, B. A. & Sansom, M. S. HOLE: a program for the analysis of the pore dimensions of ion channel structural models. *J. Mol. Graph.* **14**, 354–360, 376 (1996).
14. Van Renterghem, C. & Lazdunski, M. A new non-voltage-dependent, epithelial-like Na⁺ channel in vascular smooth muscle cells. *Pflugers Arch.* **419**(3-4):401-408 (1991).



Supplementary Fig. S1

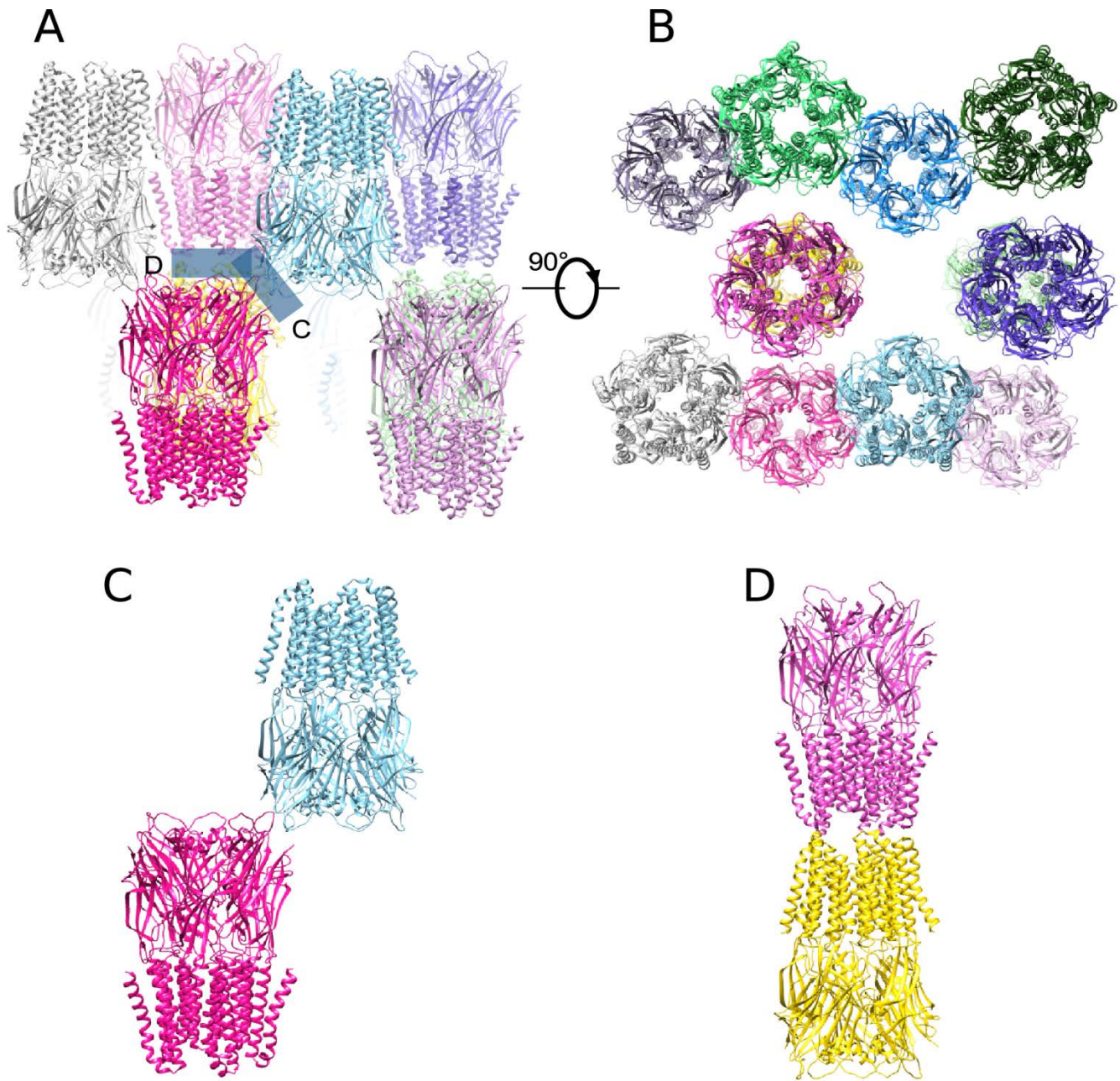
Representative electron density maps for the 2.3 Å crystal structure of sTeLIC.

A. The 2mFo-DFc electron density of one monomer is depicted in blue and contoured at a level of 1σ .

B. Two views of the TMD: one corresponding to the level of F16' (upper panel) and another at the level of L9' (lower panel), with the residues represented as sticks.

C. Enlarged side view of the M2 α -helix represented as sticks. For clarity, only two M2 α -helices are shown with residues facing the ion channel pore as well as R225/0'.

D. Zoom on the region of the M2-M3 loop from residue 245 to residue 252, with amino acids shown as sticks.



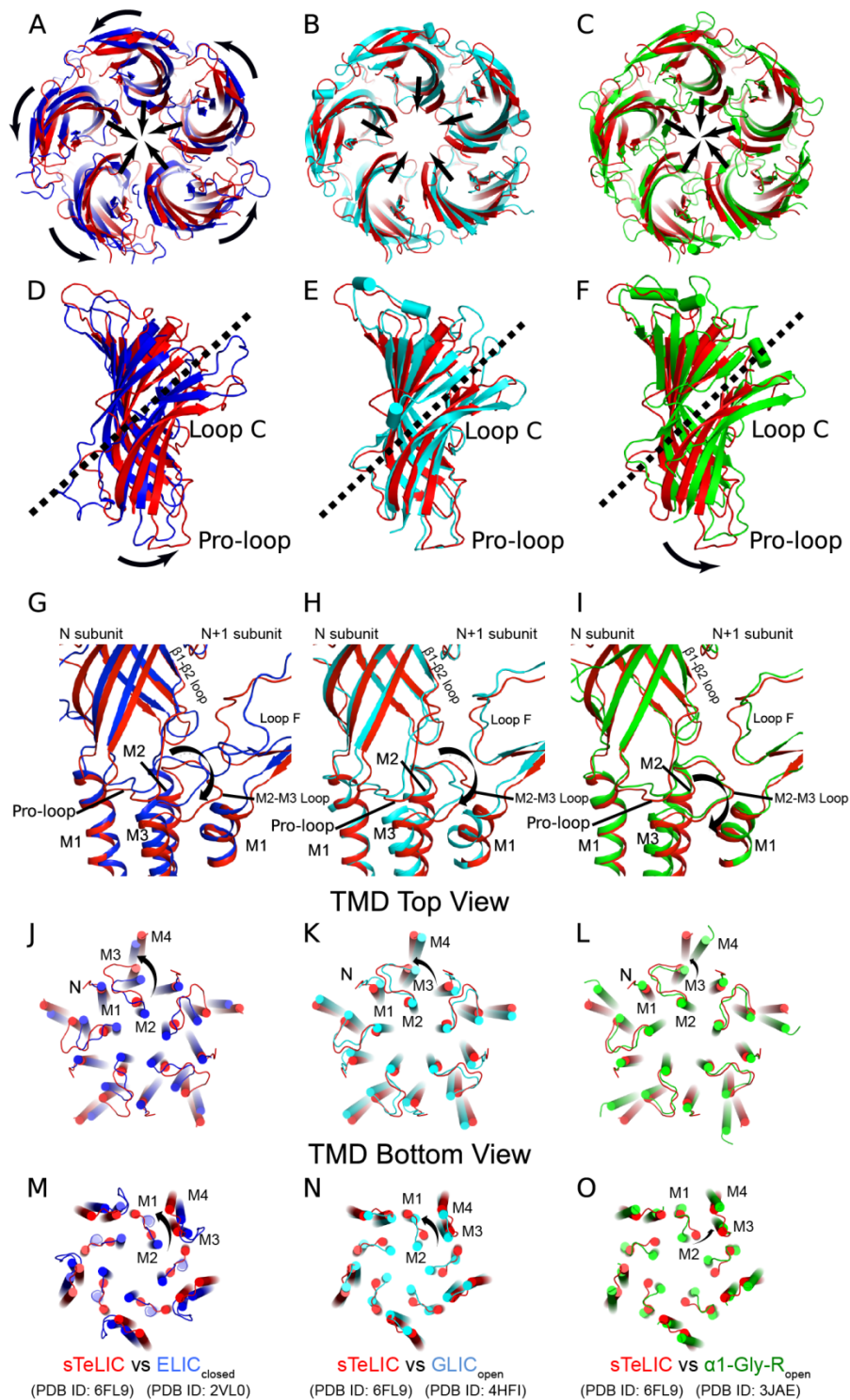
Supplementary Fig. S2

Cartoon representation of packing interactions in sTeLIC crystals.

A. View parallel to the membrane along the 5-fold symmetry axis with different pentamers shown in different colors.

B. Same as **A**, but rotated by 90 degrees, showing a view down the 5-fold symmetry axis.

C. and **D.** Details of two types of packing interactions indicated by the two blue rectangles in **A**, highlighting the main contacts between pentamers.



Supplementary Fig. S3

Detailed pairwise comparison of ECD and ECD-TMD interface of sTeLIC, ELIC, GLIC, and Gly-R.

Structural comparison of sTeLIC with bacterial and eukaryotic pGLICs, including ELIC_{closed} (PDB ID: 2VL0), GLIC_{open} (PDB ID: 4HF1) and α 1-Gly-R_{open} (PDB ID: 3JAE). TMD helices are labeled on one of the subunits.

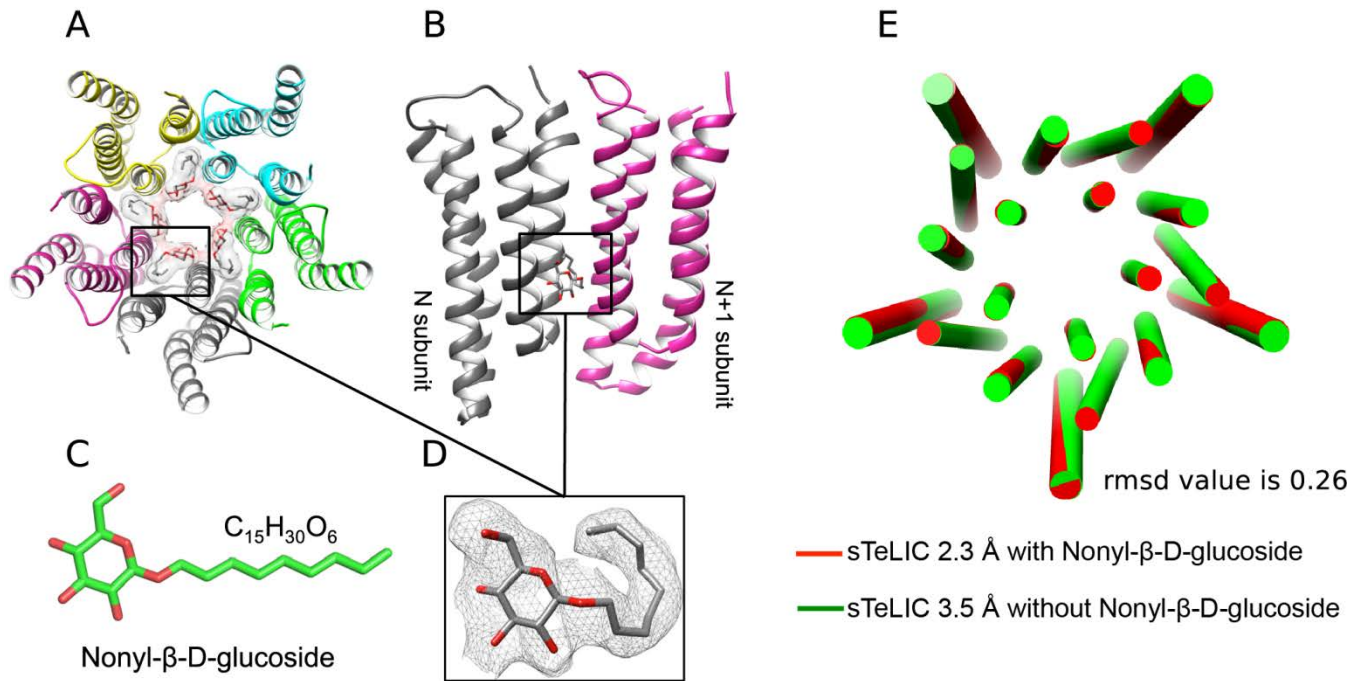
A-C. Cartoon representation of the superimposition of the TMD using the core Ca atoms to highlight the conformational change of ECD. The arrows indicate the relative movement (twist and bloom). View from the top of ECD.

D-F. View rotated by 90° to show a close-up of the ECD of one subunit.

G-I. Cartoon representation of the superimposition of the whole pentamer using the core Ca atoms to highlight the conformational change of ECD-TMD interface.

J-L. Superimposition of the ECD to highlight the change of the TMD. Top-down view of the upper TMD region.

M-O. Bottom-up view of the lower TMD-region.



Supplementary Fig. S4

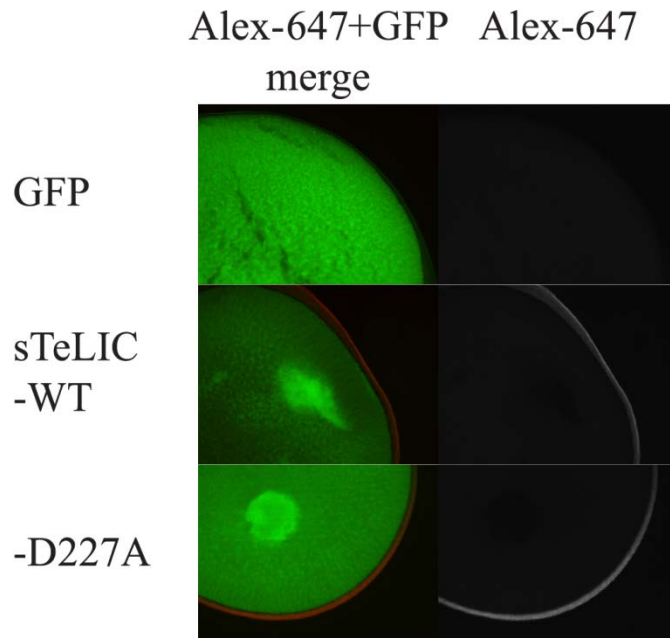
sTeLIC ion channel pore conformation with and without NDG.

A. and **B.** Top and side views depicting the position of NDG in the context of a cartoon representation of sTeLIC. NDG molecules are depicted as sticks (with van der Waals surface in **A**). The head of the NDG faces the ion channel pore and its hydrophobic tail is inserted into a crevice formed by two adjacent subunits at the level of G6'.

C. The structural and chemical formula of NDG. Oxygen atoms are in red.

D. 2mFo-DFc of Fourier electron density map shown as a gray mesh (contoured at 1 σ) with the fitted NDG molecule.

E. Superimposition of the TMD region of sTeLIC with NDG (2.3 Å resolution, red) and without NDG (3.5 Å resolution, green). The rmsd value is 0.26 Å.

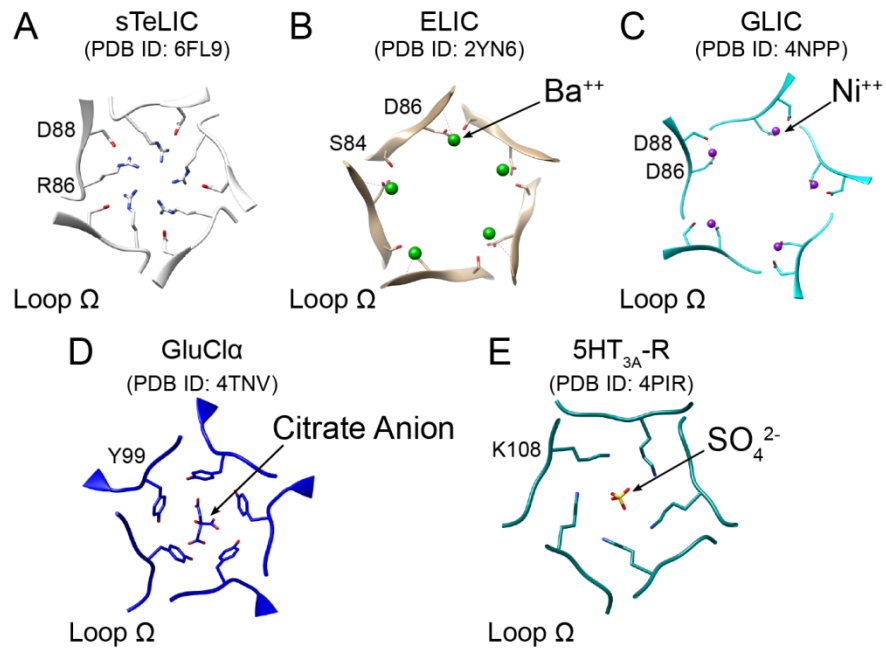


Supplementary Fig. S5

Protein expression of nonfunctional mutant D227A.

Rabbit anti-HA tag Alexa Fluor-647 immunostaining result compared to Wt and GFP-alone injected oocytes.

Left, colored merge of GFP and Alexa-647 and **Right**, the Alexa-647 imaging alone.



Supplementary Fig. S6

Common ECD constriction rings at the level of Loop Ω in various pLGICs.

A. sTeLIC (this work, PDB ID: 6FL9)

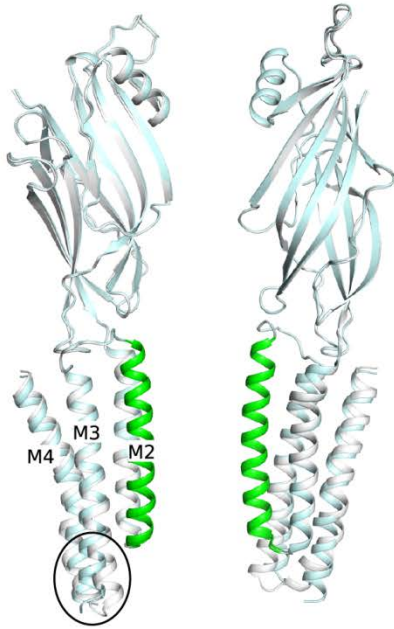
B. ELIC (PDB ID: 2YN6)

C. GLIC (PDB ID: 4NPP)

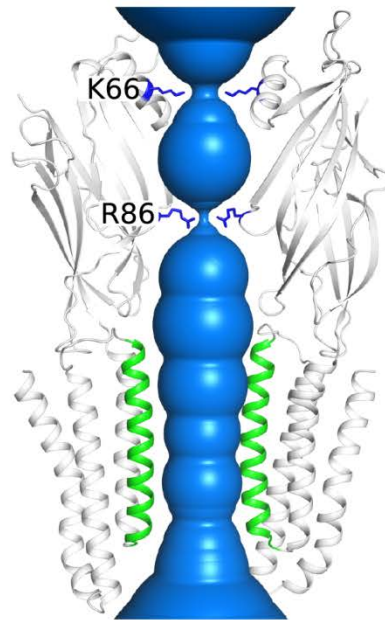
D. GluCl α (PDB ID: 4NTV)

E. 5HT $_{3A}$ -R (PDB ID: 4PIR)

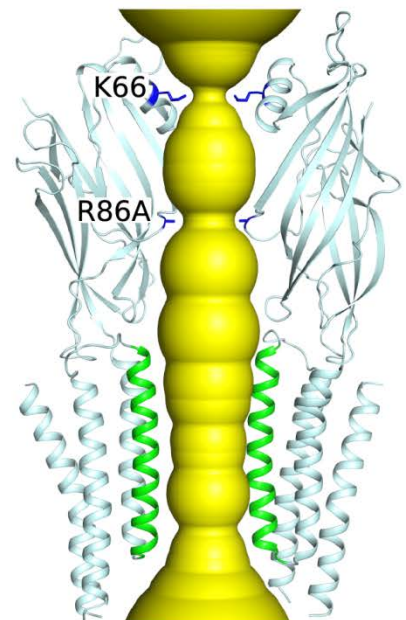
A sTeLIC wild type VS sTeLIC R86A



B sTeLIC wild type



sTeLIC R86A

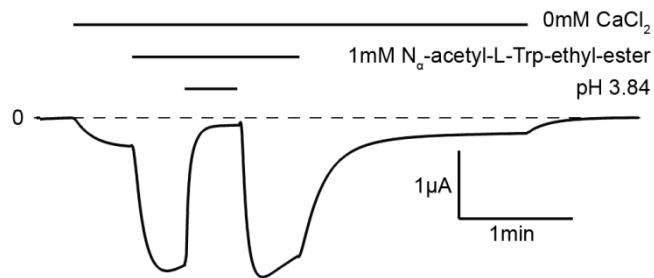


Supplementary Fig. S7

Structural characterization of sTeLIC R86A mutant.

A. Superimposition of the sTeLIC Wt (white) structure and the sTeLIC R86A mutant (palecyan). The M2 helices are highlighted as green. The overall conformation of the sTeLIC R86A mutant is the same as the wild type one, except the bottom of M3 helices and the bottom of M4 helices and their connection M3-M4 loop as indicated in the black circle.

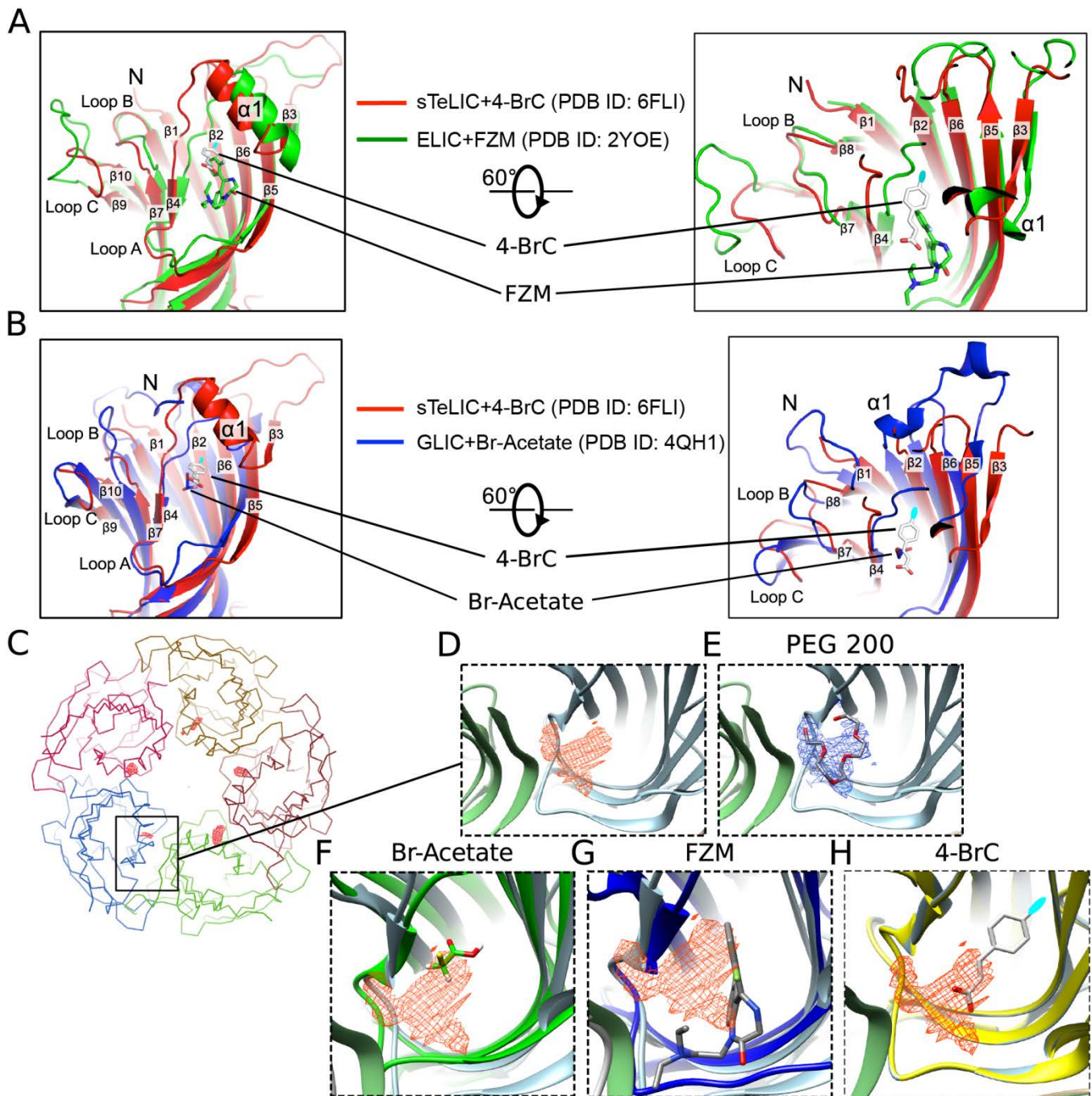
B. The solvent-accessible region from the vestibule of the ECD to the pore of the TMD in the sTeLIC Wt (Left panel, blue) and in the sTeLIC R86A mutant (Right panel, yellow).



Supplementary Fig. S8

pH modulates the channel not titratable compounds.

Perfusion of pH 7.5 standard-solution with CaCl_2 -free standard-solution elicited current, followed by 1 mM $\text{N}\alpha$ -acetyl-L-Trp-ethyl-ester potentiation, both of which are inhibited by low pH, below pH 5. This indicates pH modulation of the channel rather than the titratable compounds.



Supplementary Fig. S9

Structural comparison of the ECD vestibule PAM site.

A. Left panel: superimposition of the complex between sTeLIC and 4-BrC (this work, PDB ID: 6FLI) with the complex between ELIC and FZM (PDB ID: 2YOE). sTeLIC structure is shown in cartoon mode and colored in red. 4-BrC is depicted as sticks with the bromine atom colored in cyan and oxygen atoms colored in red. ELIC is colored in blue with FZM represented as sticks. Right panel: Rotated by 60°.

B. Left panel: superimposition of the complex between sTeLIC and 4-BrC (this work, PDB ID: 6FLI) with the complex between GLIC and Br-Acetate (PDB ID: 4QH1). GLIC is colored in green and Br-Acetate is shown in a stick representation. Right panel: Rotated by 60°.

C. Top-down view of the sTeLIC pentamer, with the additional electron density of the PAM site shown by the Fo-Fc map contoured at 3.0 σ as a red mesh.

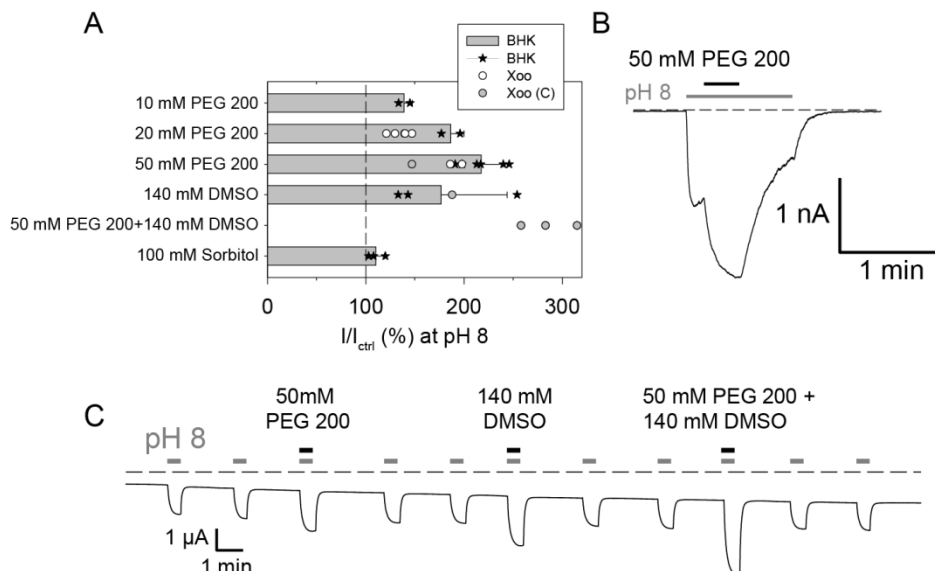
D. Enlarged view of the of additional electron density (red).

E. Same region after the tentative refinement of a PEG 200 molecule, shown as sticks with the 2mFo-DFc map overlaid and contoured at the level of 1 σ in a blue mesh.

F. Same view as in **D** with the Br-Acetate in GLIC overlaid.

G. Same view as in **D** with the FZM in ELIC overlaid.

H. Same view as in **D** with the 4-BrC in sTeLIC overlaid.



Supplementary Fig. S10

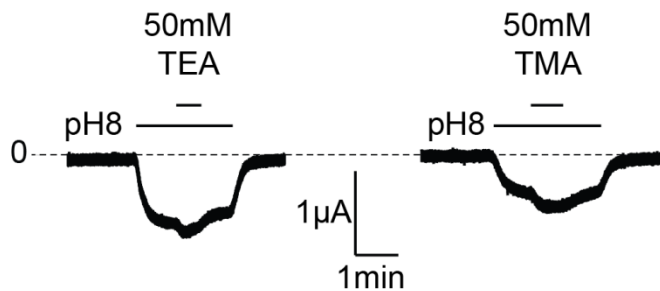
Potentiation of sTeLIC current by PEG 200 and by DMSO.

A. Bar graph with peak values of currents potentiated by 50mM PEG 200, 140 mM DMSO or 100 mM sorbitol applied at pH 8, measured as a percent of the control current at pH 8. Mean \pm standard deviation values are from whole-cell voltage-clamp experiments in BHK cells, in the protocol illustrated in **B**. Superimposed to the bars are the values obtained from individual BHK cells (stars), as well as additional data points obtained from oocytes in a similar protocol (white circles), or in a different protocol illustrated in **C** (grey circles).

B. Whole-cell voltage-clamp current trace from a BHK cell expressing sTeLIC, showing the effect of 50 mM PEG200 applied after sTeLIC activation at pH 8 (10 s).

C. Two-electrode voltage-clamp current trace from an oocyte expressing sTeLIC, showing the effect of 30 s long, direct applications of 50mM PEG 200, 140 mM DMSO (equivalent to 1% v/v), and then both simultaneously, at pH 8. Test applications are separated by two control applications at pH 8 with no added compound.

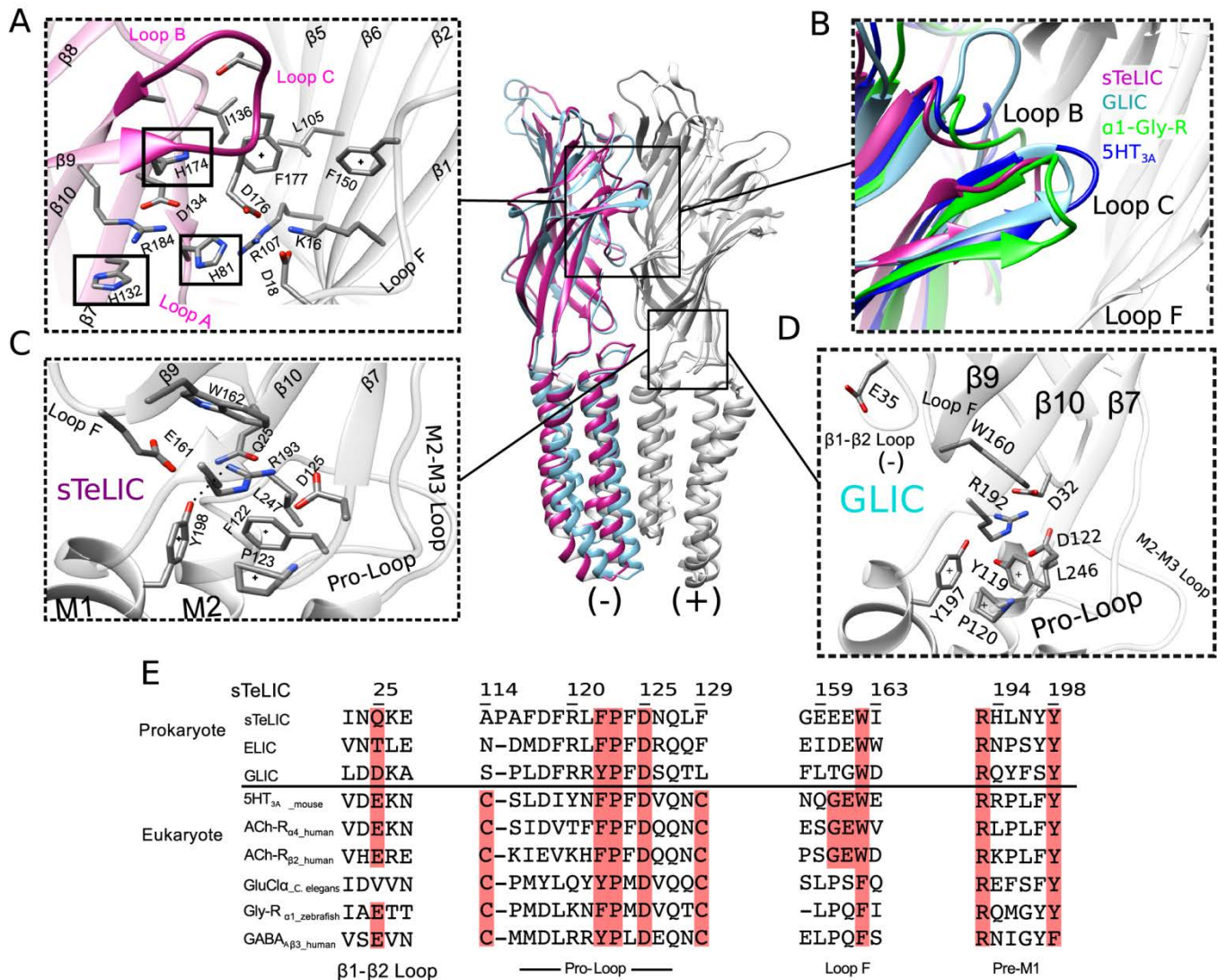
The graph in **A** includes data from 6 BHK cells and 9 oocytes, holding potential -40 mV.



Supplementary Fig. S11

Effect of quaternary ammonium ions.

Representative trace (of three oocytes tested at -40 mV) showing that pH 8 CaCl_2 -free standard-solution elicited currents are not inhibited by the presence of either 50 mM TEA or 50 mM TMA.



Supplementary Fig. S12

Structural characterization of the open-state stabilization

Central view: superimposition pentamer of sTeLIC and GLIC (PDB ID: 4HF1) structures. For clarity, only two subunits are shown. One monomer of sTeLIC is colored in red and the equivalent one in GLIC is colored in cyan.

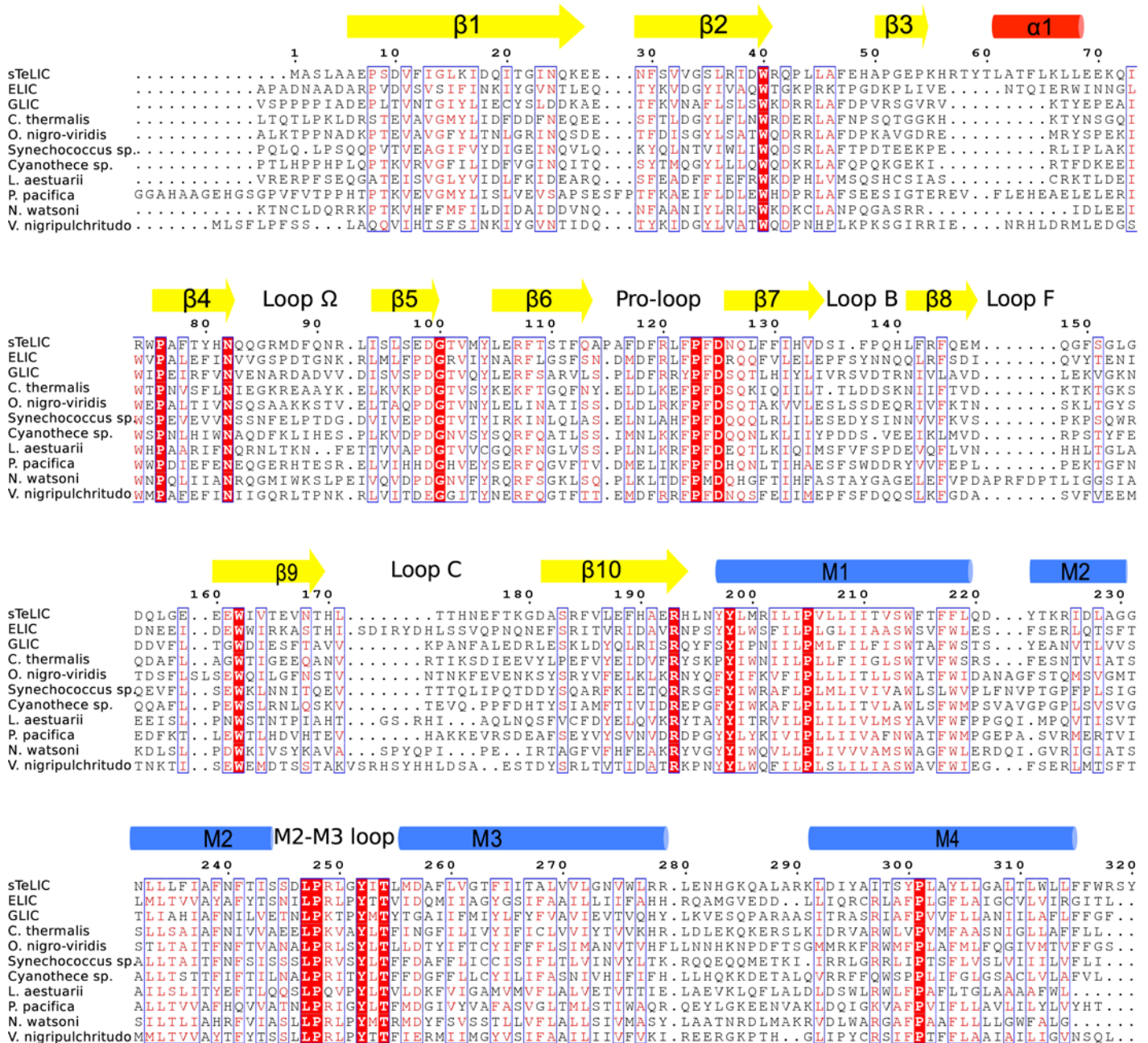
A. Inter-subunit interface of sTeLIC ECD at the level of Loop C (magenta) and Loop B. Residues surrounding the inter-subunit are shown as sticks. Histidines are framed in rectangular boxes.

B. Structural comparison of sTeLIC Loop B, Loop C (magenta) with GLIC (light blue, PDB ID: 4HF1), α 1-Gly-R (green, PDB ID: 3JAE) and 5HT_{3A}-R (deep blue, PDB ID: 4PIR).

C. Zoom on the ECD and the TMD interface and their conserved electrostatic interactions in sTeLIC, with an emphasis on the Pro-Loop, Loop F, and the M2-M3 loop.

D. Same view on GLIC.

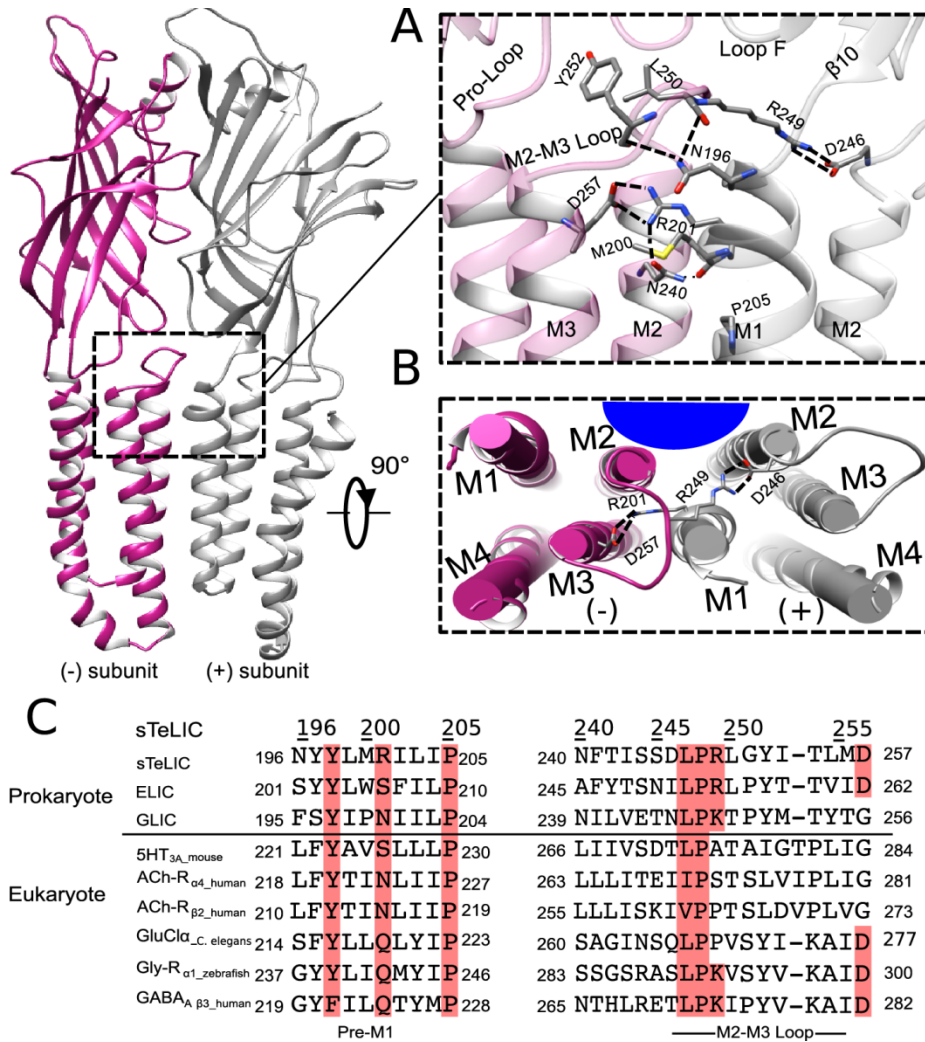
E. Sequence alignment of sTeLIC with the other members of the pGLIC family whose structure is known, focusing on the Cys loop, Loop F, Loop 2, and the pre-M1 region. Residues highlighted in panels **A-D** are boxed in red.



Supplementary Fig. S13

Sequence alignment of sTeLIC with a representative set of prokaryotic pLGICs.

ClustalW2 and ESPript were used to perform and display the alignment with the following homologs (Uniprot entry name), putting the three sequences whose structure is known on top: sTeLIC (G2FID1), ELIC (P0C7B7), GLIC (Q7NDN8), *Chroococcidiopsis thermalis* (K9U6Q3), *Oscillatoria nigro-viridis* (K9VN17), *Synechococcus sp.* (K9RYY5), *Cyanothece sp.* (B8HXN2), *Lyngbya aestuarii* (U7QEN5), *Plesiocystis pacifica* (A6FXF8), *Nitrosococcus watsoni* (D8K493), *Vibrio nigrigulchritudo* (U4EC21). The secondary structural elements of sTeLIC are indicated above the sequences. Strictly identical residues are shown in red boxes and they are also shown on the panel displaying the overall topology of sTeLIC in Fig. 1D. Well-conserved residues (with a similarity score greater than 70%) are boxed in blue and printed in red.



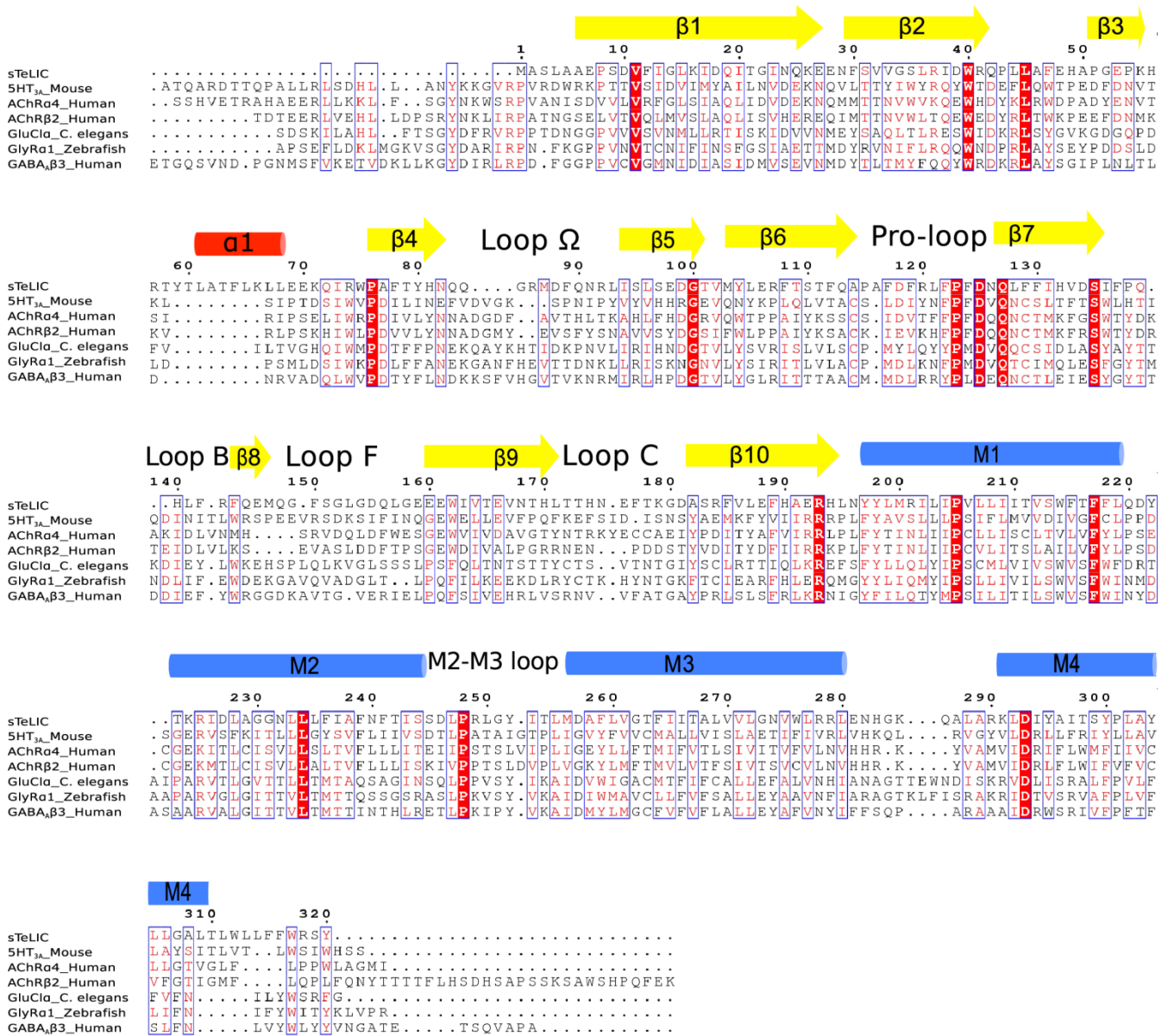
Supplementary Fig. S14

Molecular Interactions between subunits at the ECD-TMD interface.

A. Detailed view of the region of intersubunit interactions at the top of TMD. Amino acids involved in the interaction are depicted as sticks. Putative interactions and salt bridges (R249-D246, R201-D257) are shown as dashed lines.

B. Zoom on the region of interaction of M2, M3 α -helices with the adjacent M1 α -helix, viewed from the top of the TMD. The salt bridges formed by R249 (M2-M3 loop) with D246 (M2-M3 loop in adjacent subunit), D257 (top of M3 α -helix) with R201 (preM1 in adjacent subunit) in sTeLIC are indicated with a dashed line while the amino acids are shown as sticks.

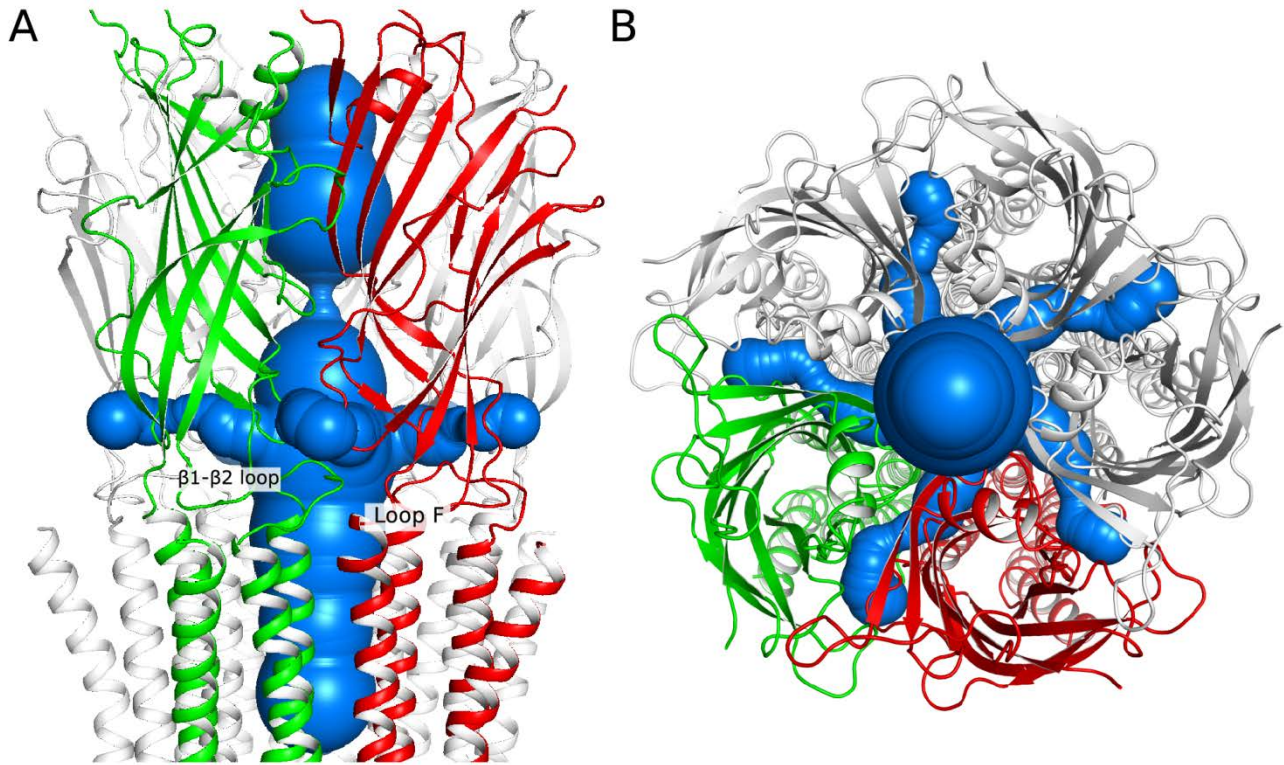
C. Sequence alignment of amino acid regions participating in the intra-subunit interaction and salt bridges at the top of the TMD of sTeLIC.



Supplementary Fig. S15

Sequence alignment of sTeLIC with eukaryotic pGLICs of known structures.

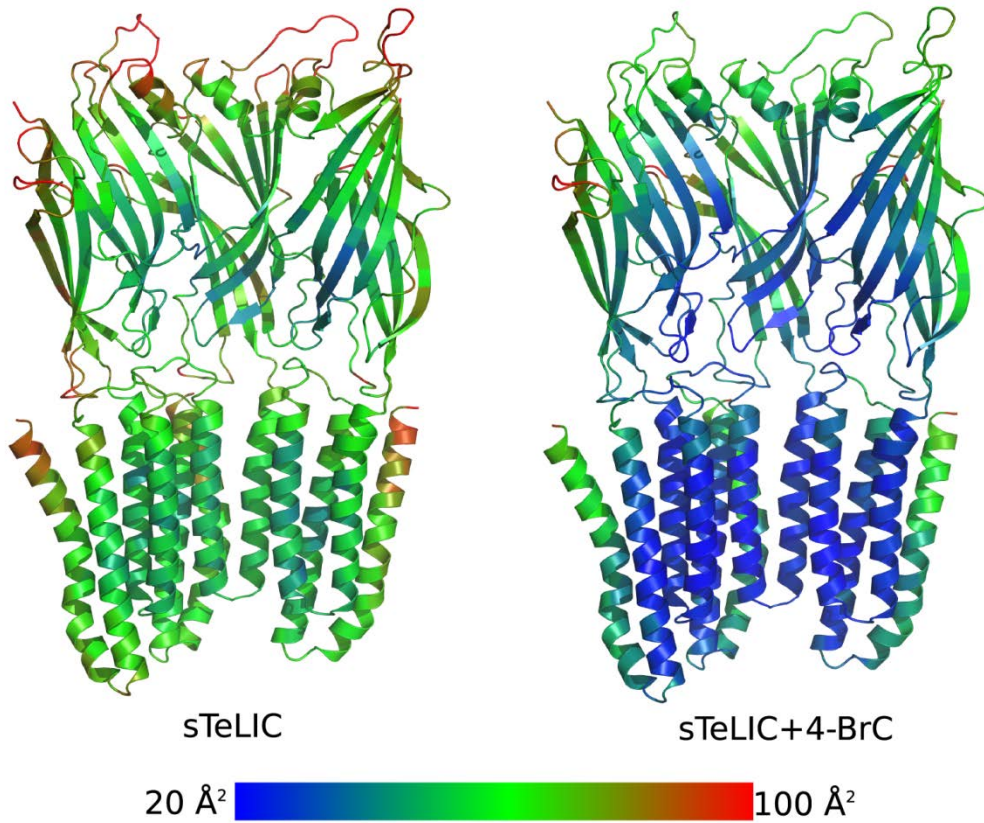
ClustalW2 and ESPrnt were used to perform and display the alignment with the following proteins sTeLIC, 5HT_{3A}_mouse, AChR $\alpha 4$ _Human, AChR $\beta 2$ _Human, GluCl α _C. elegans, GlyRa1-Zebrafish, GABA $\beta 3$ _Human. The secondary structural elements of sTeLIC are indicated above the sequences. Strictly identical residues are shown in red boxes. Well-conserved residues (with a similarity score greater than 70%) are boxed in blue and colored in red.



Supplementary Fig. S16

Possible lateral pathways for cation penetration in the lumen.

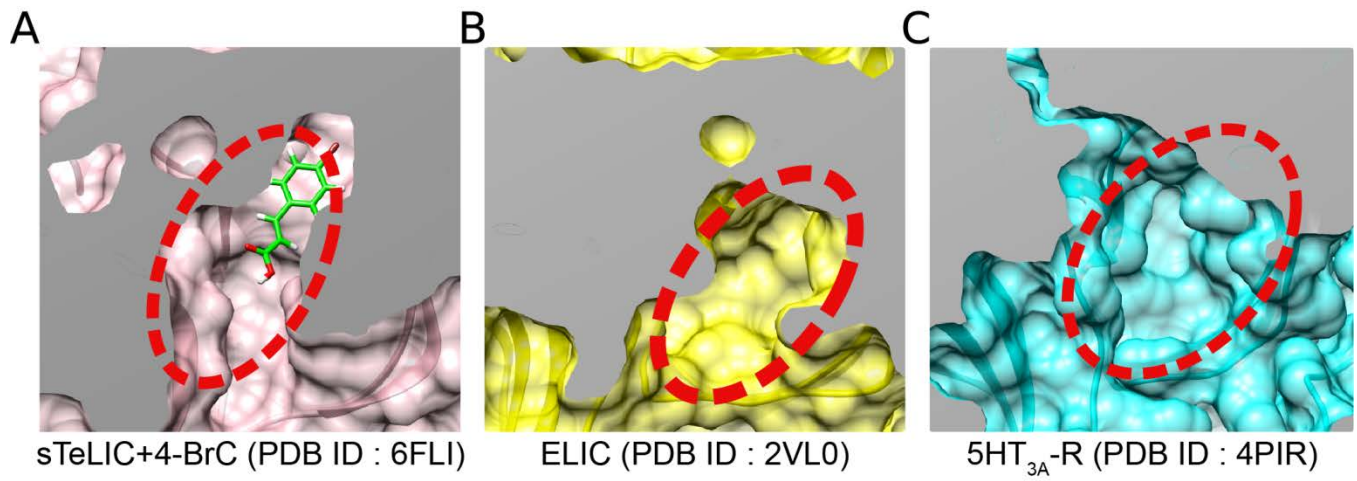
Here, the rotamers of just two residues around Loop F have been changed. **A** Lateral view. **B** Top-down view. The two subunits in front were colored in green and red. Loop F and $\beta 1$ - $\beta 2$ are highlighted.



Supplementary Fig. S17

Stabilizing effect due to the binding of 4-BrC.

The C α residues were colored according to their B-factors. With and without 4-BrC (**Right** and **Left** panels respectively).



Supplementary Fig. S18
ECD-vestibule PAM cavity comparison between selected structures.
A. sTeLIC.
B. ELIC.
C. 5HT_{3A}-R.

Supplementary Table S1

Diffraction data collection and model refinement statistics.

Structure Description (PDB ID)	sTeLIC (6FL9)	sTeLIC+4-BrC (6FLI)	sTeLIC+Cs ⁺ (6FVR)	sTeLIC+Ba ⁺⁺ (6FVS)	sTeLIC-R86A (6FVQ)
Data collection					
Beam-lines Date	Soleil PX1 18/12/2015	ESRF ID23_2 29/08/2016	Soleil PX2 24/07/2016	Soleil PX1 12/06/2016	Soleil PX1 02/12/2017
Wavelength (Å)	0.9780	0.8720	2.1000	2.0000	0.9785
Oscillation range (°)	0.10	0.15	0.2	0.1	0.1
Data processing					
Resolution (Å)	49.34-2.30 (2.34-2.30)	49.32-3.00 (3.07-3.00)	48.49-4.20 (4.49-4.20)	49.07-3.20 (3.30-3.20)	49.15-3.30 (3.42-3.30)
Space group	C 1 2 1	C 1 2 1	C 1 2 1	C 1 2 1	C 1 2 1
Cell parameters (Å, °)	219.6 113.0 144.4 90 112.1 90	222.7 112.7 144.8 90 111.2 90	221.2 114.1 144.3 90 111.8 90	218.8 112.1 144.1 90 112.8 90	216.2 112.5 144.5 90 113.8 90
R _{merge} (%)	7.1(58.5)	7.1(93.5)	12.2(99.1)	5.2(34.2)	8.7(141.0)
Reflection measured	499194(22698)	444411(30905)	255049 (47002)	166241(14462)	262566(26355)
Reflection unique	144663(7079)	66506 (4454)	24499(4443)	52251(4511)	47694(4605)
I/sigma	6.4(1.4)	8.5(1.1)	6.3(1.2)	9.1(1.9)	8.8(1.0)
Multiplicity	3.4(3.2)	6.7(6.9)	10.4(10.6)	3.2(3.2)	5.5(5.7)
CC ½ (%)	99.7(42.6)	99.9(91.1)	99.9(92.1)	99.8(95.3)	99.9(78.8)
Completeness (%)	99.7(98.8)	99.3(99.0)	99.7(99.8)	98.4(99.1)	99.7(99.4)
Model refinement					
Resolution (Å)	20.00-2.30	20.00-3.00	20.00-4.20	20.00-3.20	20.00-3.30
R _{work} /R _{free} (%)	0.21/0.24	0.19/0.22	0.24/0.24	0.21/0.23	0.21/0.22
RSMD bond lengths (Å)	0.010	0.010	0.008	0.010	0.009
RSMD bond angles (°)	1.09	1.14	1.03	1.16	1.07
No. protein atoms	12830	12810	12830	12805	12755
No. of ligand	5	10	16	7	5
No. of water molecules	477	106	-	187	-
B factor overall (Å)	72.80	49.53	75.00	64.08	71.86
B factor ligand (Å)	85.67	79.78	82.97	75.91	106.6
B factor water (Å)	41.18	23.59	-	28.33	-
Ramachandran preferred (%)	97.7	97.4	99.0	99.0	98.7
Ramachandran outlier (%)	0	0	0	0	0
Molprobrity score*	99 th	100 th	100 th	100 th	100 th

*100th percentile is the best among structure of comparable resolution; 0th percentile is the worst.

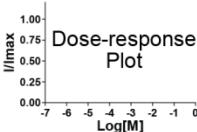
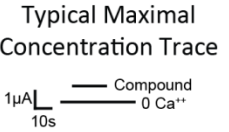

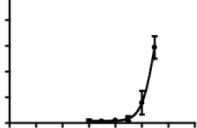
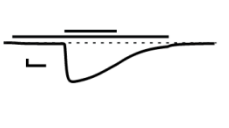
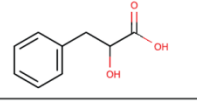
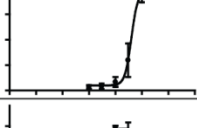

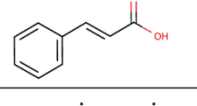
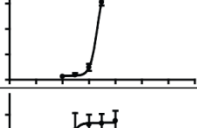
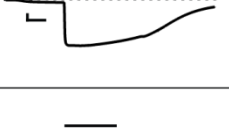
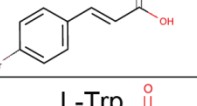
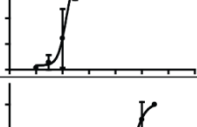
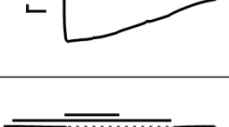
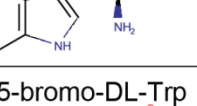
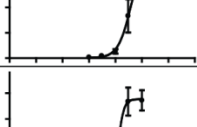


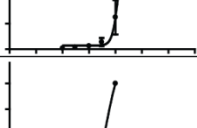

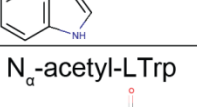
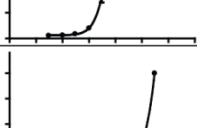

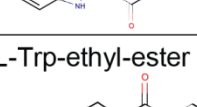
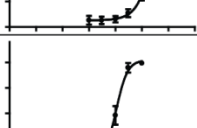

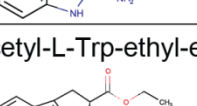
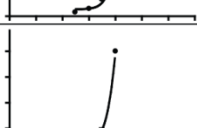
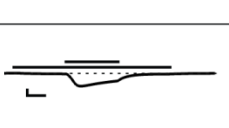
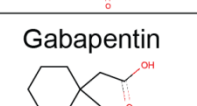
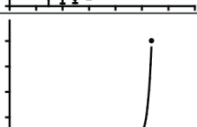
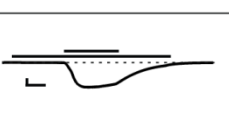
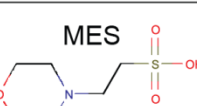
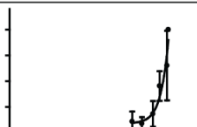
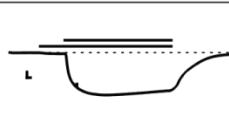



Supplementary Table S2: Various compounds tested, that are of general interest for the pLGIC family, which had little or no effect.

Compounds were tested at the maximal concentration indicated at pH 7.5 in the absence (left) or presence (right) of a positive allosteric modulator (PAM). No effect was observed except for compounds with a bolded font, signifying a small but robust potentiating effect at the concentration indicated.

Left: Standard solution (or ** CaCl₂ free standard solution). *Right:* Standard solution with 30 mM MES (or ** CaCl₂ free standard solution with 10 μM 4-BrC).

Compound	[mM]	[mM] w/ PAM
5-HT	5	5
Acetylcholine	30	30
β-Alanine	10	-
Caffeic Acid	10**	-
Citric Acid	1.8	-
DMSO	(1% v/v)**	(1% v/v)**
GABA	30	30
L-Glutamate	30	30
L-Glycine	30	30
L-Histidine	30**	-
Histamine	30**	10
HEPES pH 7.5	30	30
Ivermectin	0.5	0.5
IPTG	1**	-
L-Leucine	30**	30**
Levodopa	10**	-
L-Methionine	30**	30**
Nicotine	0.35	-
PEG 200	30**	30**
Picrotoxin	0.1**	0.1**
L-Serine	30**	30**
Mixture of Sugars (Glucose, Sucrose, Maltose)	5**	5**
Taurine	30	-
Tris-HCl pH 7.5	30	-
L-Tyrosine	1**	-

Supplementary Table S3: Dose-response values for amino-acid derivatives found to display a potentiating effect at pH 7.5.

Compound	EC ₅₀ [mM]	Dose-response Plot 	Typical Maximal Concentration Trace 
	Hill-slope		
	I _{max} (μA) (n)		
L-Phe 	>10		
	ND		
	-5 ± 3 (4)		
DL-3-Phenyllactic acid 	4 ± 2		
	5 ± 3		
	-6.8 ± 0.4 (3)		
Trans-cinnamic acid 	0.2 ± 0.02		
	3.3 ± 0.4		
	-8 ± 0.5 (3)		
4-bromo-cinnamic acid 	0.021 ± 0.008		
	2.5 ± 0.5		
	-8 ± 2 (6)		
L-Trp 	5 ± 3		
	2.1 ± 0.6		
	-7 ± 1 (3)		
5-bromo-DL-Trp 	1.6 ± 0.6		
	2.8 ± 0.2		
	-7 ± 3 (3)		
Trans-3-indoleacrylic acid 	0.6 ± 0.2		
	1.7 ± 0.4		
	-8 ± 1 (3)		
N_α-acetyl-LTrp 	>10		
	ND		
	-5.2 ± 0.7 (3)		
L-Trp-ethyl-ester 	1.1 ± 0.2		
	2.11 ± 0.05		
	-6 ± 1 (3)		
N_α-acetyl-L-Trp-ethyl-ester 	>10		
	ND		
	-3 ± 2 (4)		
Gabapentin 	>30		
	ND		
	-5 ± 0.5 (3)		
MES 	>30		
	ND		
	-5 ± 1 (6)		